ACS APPLIED MATERIALS & INTERFACES

Research Article

www.acsami.org

Variation in Optoelectronic Properties of Azo Dye-Sensitized TiO_2 Semiconductor Interfaces with Different Adsorption Anchors: Carboxylate, Sulfonate, Hydroxyl and Pyridyl Groups

Lei Zhang,[†] Jacqueline M. Cole,*[,†,‡] and Chencheng Dai[§]

[†]Cavendish Laboratory, University of Cambridge, J. J. Thomson Avenue, Cambridge CB3 0HE, United Kingdom

[‡]Argonne National Laboratory, 9700 South Cass Avenue, Argonne, Illinois 60439, United States

[§]Department of Chemical Engineering, University of Cambridge, New Museums Site, Pembroke Street, Cambridge CB2 3RA, United Kingdom

Supporting Information

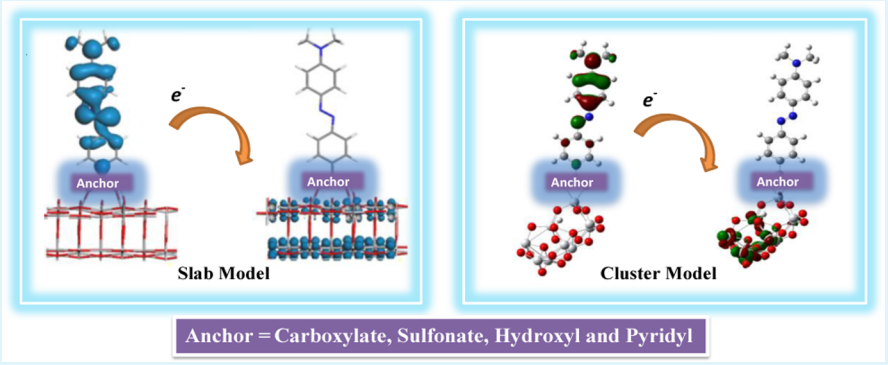

ABSTRACT: The optoelectronic properties of four azo dye-sensitized TiO_2 interfaces are systematically studied as a function of a changing dye anchoring group: carboxylate, sulfonate, hydroxyl, and pyridyl. The variation in optoelectronic properties of the free dyes and those in dye/TiO_2 nanocomposites are studied both experimentally and computationally, in the context of prospective dye-sensitized solar cell (DSSC) applications. Experimental UV/vis absorption spectroscopy, cyclic voltammetry, and DSSC device performance testing reveal a strong dependence on the nature of the anchor of the optoelectronic properties of these dyes, both in solution and as dye/TiO_2 nanocomposites. First-principles calculations on both an isolated dye/TiO_2 cluster model (using localized basis sets) and each dye modeled onto the surface of a 2D periodic TiO_2 nanostructure (using plane wave basis sets) are presented. Detailed examination of these experimental and computational results, in terms of light harvesting, electron conversion and photovoltaic device performance characteristics, indicates that carboxylate is the best anchoring group, and hydroxyl is the worst, whereas sulfonate and pyridyl groups exhibit competing potential. Different sensitization solvents are found to affect critically the extent of dye adsorption achieved in the dye-sensitization of the TiO_2 semiconductor, especially where the anchor is a pyridyl group.

KEYWORDS: *dye-sensitized solar cell, first-principles, DFT, TDDFT, nanoparticles, anchor, azo, pyridyl, carboxylate, sulfonate, hydroxyl*

INTRODUCTION

Dye-sensitized solar cells (DSSCs) are a strong contender as a next-generation solar-cell technology for clean energy applications.[1−4] In particular, their transparent device attributes make them attractive as photovoltaic "smart windows".[5−7] Such devices employ chemical dyes to capture the solar energy, and convert photons to electrons once they have been adsorbed onto the surfaces of appropriate metal oxide nanoparticles. The majority of dyes used in DSSCs are based on ruthenium complexes; even though there is currently a trend towards using perovskite-based organometallics.[8−13] Nevertheless, organic dyes still enjoy a number of advantages such as their molecular tunability, lower cost, easier synthesis, and material abundance.[14−17] As a result, continuing efforts should be maintained on developing organic dyes for DSSCs and understanding their associated structure−property relationships.

To be DSSC-active, a dye molecule must contain a chemical substituent that can anchor the chromophore onto the metal oxide via adsorption. The dye itself provides the innate solar light harvesting properties of the DSSC, while its chemisorption onto the metal oxide (usually TiO_2) nanoparticles creates an interfacial path by which electrons can be transferred from the

Received: February 11, 2014
Accepted: May 2, 2014
Published: May 2, 2014

dx.doi.org/10.1021/am502186k | ACS Appl. Mater. Interfaces 2014, 6, 7535−7546

organic dye to the bulk semiconductor; this interfacial electron injection initiates the electrical current in a DSSC. The nature of the anchoring group employed is therefore a very important consideration for DSSC device functionality. Various anchoring groups have been successfully demonstrated in these devices, e.g., carboxylate, phosphonate, sulfonate, salicylate, 8-hydroxylquinoline, acetylacetonate, catechol, hydroxyl, pyridyl, and hydroxamate.[18−22] Despite the importance of their anchoring abilities within a DSSC,[23−32] there is a disproportionate dearth in systematic investigations that comprehensively assess their relative impact in this photovoltaic technology.

This study seeks to offset this lack of information via a systematic survey of the relative influence of four azo dyes on the optoelectronic properties of dye/TiO_2 nanoparticles and the associated dye in solution. The four azo dyes, sharing a common dialkylamino-phenyl-diazenyl molecular framework, bear four different end groups: benzoic acid, sulfonoic acid, phenol, and pyridine; this provides a four-way systematic variation in their associated anchoring groups (carboxylate, sulfonate, hydroxyl and pyridyl) by which one can perform the required comparisons. The dyes are otherwise chemically identical, except for the case where the pyridyl anchor is involved; there, ethyl rather than methyl groups lie in the electron donor region of the molecule, owing to practical limitations of sample availability. Fortunately, it is known from previous work that optoelectronic properties of such azo dyes bearing these two different alkyl groups have negligible impact on their optoelectronic properties, although their crystal structures differ dramatically.[33]

Azo dyes were selected for this study because they are widely available and cost effective.[34−36] They form one of the largest family of industrial dyes; however, their performance in DSSCs are much less investigated and there is plenty of room for improvement. As a result, the interfaces formed between the azo dyes and TiO_2 metal oxide should be studied, in order that we can molecularly engineer them in certain ways to make azo dyes perform better in optoelectronic devices.

The exact chemical specifications of the dyes, [(E)-4-((4-(dimethylamino)phenyl)diazenyl)benzoic acid, **1**], [(E)-4-((4-(dimethylamino)phenyl)diazenyl)benzenesulfonic acid, **2**], [(E)-4-((4-(dimethylamino)phenyl)diazenyl)phenol, **3**] and [(E)-*N*,*N*-diethyl-4-(pyridin-4-yldiazenyl)aniline, **4**] are displayed in Scheme 1, with their anchor highlighted.

The systematic study proceeds by first assessing the optical and electronic properties of the dyes in solution (the "free dyes"). Secondly, the optoelectronic effects of dyes anchored onto TiO_2 nanoparticles are probed. Lastly, the dye-incorporated DSSC device performance is tested to probe their photovoltaic attributes. During the course of this study, attention is also drawn to the two computational models used to model the dye···TiO_2 interface: one based on an isolated dye/TiO_2 cluster and the other based on a dye located on the surface of a 2D periodic slab of TiO_2.

EXPERIMENTAL AND COMPUTATIONAL METHODS

Materials. **1**, **3** and **4** were supplied by TCI while **2** was purchased from Sigma-Aldrich and used without further purification.

Dye/TiO_2 Film Fabrication. Solvent-modified dye/TiO_2 films were prepared according to the same steps to fabricate the working electrodes (vide infra). Both dimethyl sulfoxide (DMSO) and the commonly used 1:1 acetonitrile/tert-butanol solvent were used as the sensitizing solvent. The electrodes were sensitized in the dye solution for 24 h and 15 min, respectively. The presence of DMSO enabled the effect of polar solvent intervention on dye take-up and coverage on TiO_2 film to be probed. Before the optical spectroscopy measurements were performed, the films were rinsed in ethanol to remove excessive unadsorbed dyes and dried with N_2.

Scheme 1. Molecular Structures of 1−4, Which Have Carboxylate, Sulfonate, Hydroxyl, and Pyridyl Anchors, Respectively[a]

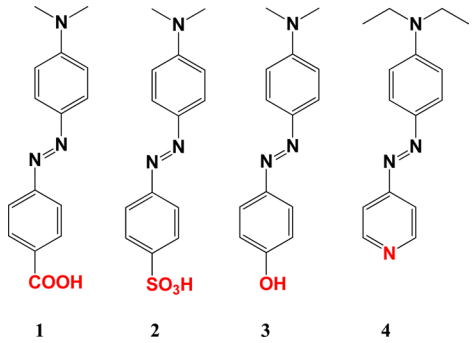

[a]Only the anchors are allowed to change, except for **4**, where the alkylamino group also differs. The anchoring moieties employed to interact with TiO_2 nanoparticles are highlighted in red.

Optical Spectroscopy. The UV/vis absorption spectra of both solution-based free dyes (either in 1:1 acetonitrile/tert-butanol or DMSO) and film-based dye/TiO_2 nanocomposites were determined using an Agilent8453 diode array spectrophotometer. The uncertainty in the UV/vis measurement is 2 nm.

Electrochemical Characterization. Cyclic voltammetry (CV) data were determined in a N_2-saturated three-electrode system, where the working, counter and reference electrodes are glassy carbon, platinum and Ag/AgCl/3.0 M KCl, respectively. The glassy carbon electrode was polished with 1.0 μm alumina slurry (Buehler) and then sonicated for 10 min in Milli-Q water (Millipore). The organic dyes were dissolved into DMSO with 0.1 M tetrabuylammonium perchlorate (TBAP) as the supporting electrolyte. The scan rate was 100 mV/s. The Ag/AgCl reference electrode was calibrated using a ferrocene/ferrocenium (Fc/Fc^+) redox couples as an external standard.

DSSC Device Fabrication and Testing. Although the in-house DSSC performance characteristics for **1** has been reported before,[33] they are included in this paper, as a reference. **1** was fabricated and characterized under the same conditions as **2**-**4**. This involved a single TiO_2 layer (DSL 18NR-T, Dyesol) being deposited onto the FTO glass (TEC15, Dyesol) via the doctor-blade method; this layer is ca. 4 μm, formed from TiO_2 particles each bearing a size of ca. 20 nm. The resulting electrode was sintered at 500 °C for 30 min. The film was sensitized in 0.5 mM dye solution with 1:1 acetonitrile/tert-butanol overnight to obtain the working electrodes. The counter-electrodes were prepared using chloroplatinic acid hexahydrate ($H_2PtCl_6{\cdot}6H_2O$, Sigma). A 50 μm thick thermoplastic film of Surlyn (Solaronix) was used to separate the two electrodes, and the cavity was filled with an electrolyte consisting of a 50 mM iodide/tri-iodide redox couple (HPE, Dyesol). At least five duplicate cells for each dye were fabricated and tested (see Table S1 in the Supporting Information) to ensure adequate consistency of the DSSC results which is particularly important given their modest DSSC efficiency.

The current−voltage (J−V) characteristic responses and the overall DSSC efficiencies were determined using an ABET Sun 2000 solar simulator under AM1.5 illumination at 100 mW cm^{-2}, after spectral mismatch. Errors were maintained within 6% for overall efficiency (η), short circuit current (J_{sc}), open circuit voltage (V_{oc}), and fill factor (FF). The external quantum efficiency (EQE) was quantified by illuminating the DSSC with a spectrally resolved halogen lamp, calibrated by a silicon diode.

Quantum Calculations of Dye/TiO_2 System: General Model Considerations. Modelling the real mesoporous structure of dye/

TiO_2 nanocomposites in a DSSC requires an extremely large computational cost. To simplify the modelling process, we herein used two methods, which differ principally in whether a cluster or a solid-state periodic condition is employed, to understand the working electrode of a DSSC.

In this study, Method 1 models dye/TiO_2 as an isolated nanocomposite cluster; the associated DFT calculations are based on a localized basis set; this method is widely used in the literature for studying dye···TiO_2 interfaces.[37−43] A small TiO_2 cluster $(TiO_2)_n$ (n is generally <80) is typically considered. This small cluster size has been shown to be sufficient for optoelectronic property calculations on TiO_2 and dye/TiO_2 nanocomposites for DSSC applications.[44,45] The other method presented herein, Method 2, considers the other extreme: a periodic condition is employed to model infinitely large particles in one (1D) or multiple dimensions (2D), using plane wave basis sets.

Both methods have pros and cons. For example, Method 1 is more powerful when solvent effects should be considered, but it is less applicable to larger TiO_2 nanoparticles and the "edge effect" is exaggerated. Method 2 is similar to the real world scenario where the mesoporous structure consists of a large array of connected anatase nanocrystals, even though its inherent 2D structure is not essentially "mesoporous". In this article, we therefore engage both an isolated cluster and a periodic dye/TiO_2 slab to model the DSSC system, in order to offer a more comprehensive view of the dye/TiO_2 interactions introduced by the anchoring groups.

Computational Details for the Isolated Dye/TiO_2 Model (Method 1). Calculations of all isolated dye/TiO_2 structures used localized basis sets and were carried out in GAUSSIAN 09 software.[46] The dye/TiO_2 system is based on a cluster size, $(TiO_2)_9$;[44,45] this size reflects a balance between computational cost and a realistic nature of the results. Indeed, Sánchez-de-Armas et al.[44] have studied the computational size effect of TiO_2 and found that $(TiO_2)_9$ is large enough to replicate the real electronic properties of anatase structures. The $(TiO_2)_9$ cluster has also been employed to study anchoring effects,[45] and the same $(TiO_2)_9$ cluster has been found to produce similar anchoring modes with experiments. In addition, even when using a larger cluster such as the example of $(TiO_2)_{38}$ (ca. 1−2 nm on edge),[47,48] this size is still more than ten times smaller than the real nanoparticle size for DSSCs presented in the experimental aspects of this study (ca. 20 nm on edge). Structural optimizations of the ground state were performed by hybrid density functional theory (DFT), using a B3LYP functional[49] and a 6-31g(d,p) basis set.[50] Following geometrical optimization, the associated vibrational frequencies were calculated to ensure that they were all positive, so as to avoid unrealistic saddle points. In addition to performing the calculation in vacuo, solvent effects on the structures were also studied by employing the polarizable continuum model (PCM)[51] in both acetonitrile and DMSO.

Time-dependent density functional theory (TDDFT) was employed to understand the different effect of each anchoring group on the optical properties of the dye/TiO_2 cluster, at optimized geometry given by DFT. Simulated UV/vis absorption spectra were calculated in Gaussian09,[46] and visualized in GaussView.[52] In common with the ground-state calculations, the excited-state calculations were performed in vacuo, and in DMSO and acetonitrile solvents. Absorptivity, ε, can be derived from oscillator strengths,[53] that are obtained from TDDFT calculations. Because of the large molecular system being modeled, the UV/vis absorption spectra of the dye/TiO_2 composites were generated using 30 states (n_{states} = 30).

Molecular energy levels and distributions, including highest occupied molecular orbital (HOMO) and lowest unoccupied molecular orbital (LUMO), as well as HOMO−1 and LUMO+1, were determined using the optimized structure. The adsorption energy of the dye/TiO_2 system was estimated from

$$E_{adsorption} = E_{dye} + E_{TiO_2} - E_{dye/TiO_2}$$

Computational Details for the Dye/TiO_2 Periodic Model (Method 2). A 2D slab of the TiO_2 nanostructure was constructed by cutting the anatase (101) surface in a similar way to that of previous studies.[54,55] The supercell corresponds to a surface area of 11.394 Å × 10.513 Å. The vacuum layer is 20 Å to enforce minimum interaction between different slabs. For each slab, the thickness is ca. 7 Å. The bottom layer of the slab is constrained, while the other layers and dyes are allowed to relax. The geometrical optimization (GO) was performed using CASTEP in Materials Studio[56] at the Γ-point, due to the large size. The cutoff energy was set to 340 eV, using an ultrasoft pseudopotential and a PBE functional.

The absorption coefficients, $\alpha(\omega)$, of the dye/TiO_2 system were obtained from the dielectric constants calculated at the corresponding optimized structures, using the same cutoff energy (340 eV), PBE functional and ultrasoft pseodopotential for Ti, O, C, N and H, as used for the geometrical optimization. The optical properties were averaged over all polarization directions, thereby imitating a polycrystalline sample.

The anchoring modes of the carboxylic acid have been evaluated theoretically in the literature.[20,54,57−60] These modes can be either dissociative or nondissociative, depending on whether the hydrogen remains as a part of the dye or if it is transferred as a proton to the TiO_2 surface. Seven different adsorption modes for **1** were calculated via both Method 1 and Method 2 to identify the stable anchoring modes (see Scheme S1 and Table S2 in the Supporting Information) for the carboxylic acid anchor. The anchoring modes in the upper row (MHa, MHb, BH, and BBH) have a nondissocative anchoring mode. The anchoring modes in the bottom row [M(H), B(H) and BB(H)] have dissociative anchoring modes. Both methods predict bidentate modes to be stable for **1**, although Method 2 suggests bidentate bridging to be more stable while Method 1 prefers the bidentate chelating mode (see Table S2 in the Supporting Information).

The literature lacks a detailed theoretical anchoring mode evaluation of the sulfonate, hydroxyl and pyridyl groups. Based on the anchoring calculation of the carboxylic acid, similar anchoring modes were used as the starting point for geometrical optimization of the sulfonic acid anchor. The third coupling site for the five-fold titanium atom of the tridentate anchoring mode of the sulfonate was not available in the 2D model; as a result, a bidentate bridging anchoring mode, stabilized by a hydrogen-bond (HB) with a six-fold titanium atom at the surface, was presumed for the sulfonate anchor in this case. This assumption is reasonable also because the phosphoric acid anchor, which has similar structure as the sulfonic acid, exhibits a stable bidentate bridging anchoring mode from density functional theory calculations.[61] Dissociated modes with chemical bonding between an unsaturated titanium atom and a hydroxyl oxygen in **3**, and pyridine nitrogen for **4**, were used as suggested by previous research.[18]

The calculated band gap from Method 1 and Method 2 should be used with caution in this study, where the combined dye/TiO_2 system is concerned, rather than those of the individual components. A small "band gap" of such a combined system does not necessarily imply a red-shifted UV/vis absorption peak as the associated oscillator strengths for these transitions are likely to be small. Rather, this observation is a good indicator of structure and properties at the dye/TiO_2 interface.[55]

Quantum Calculations for the Nonadsorbed "Free Dyes". The technical details of the DFT and TD-DFT calculations on the free dyes, using localized basis sets, are the same as those for the isolated cluster dye/TiO_2 modelling. The properties were similarly examined in vacuo and in DMSO and acetonitrile solvents.

The free dyes were also modelled within the periodic boundary condition, in order to enable their adsorption energies to be determined. These calculations employed a supercell of the free dyes, constructed in the same way as for the dye/TiO_2 nanocomposites.

RESULTS AND DISCUSSION

UV/Vis Absorption Characteristics of 1−4. The peak UV/vis absorption wavelength and the associated absorptivity are important indicators of the light harvesting capacity of DSSC dyes. From experimental UV/vis absorption spectros-

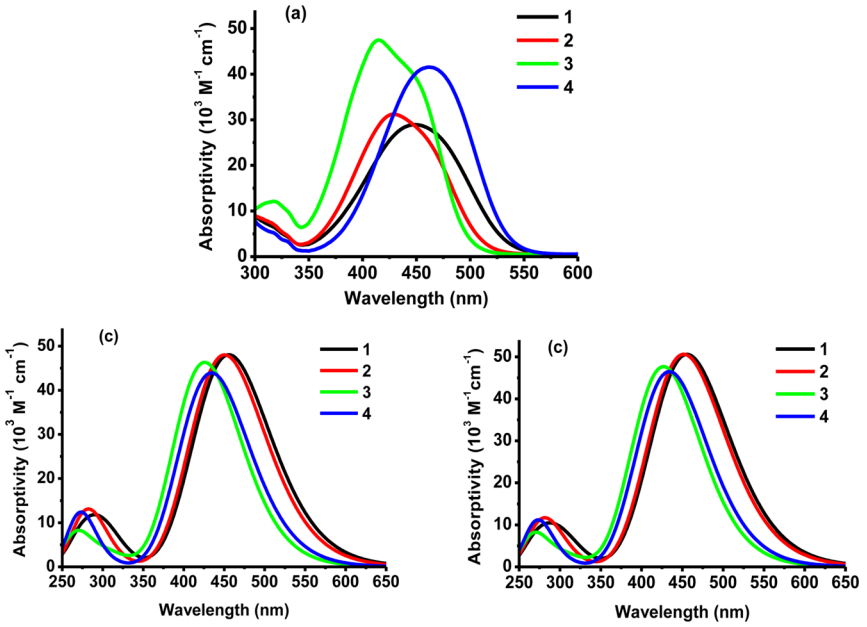

Figure 1. (a) Experimental UV/vis absorption spectra of **1**, **2**, **3**, and **4** in DMSO solution. (b) UV/vis absorption spectra of **1**−**4** simulated by TDDFT calculations in vacuo. (c) UV/vis absorption spectra of **1**−**4** simulated by TDDFT in DMSO solution.

copy in DMSO (Figure 1a), **1** (carboxylate anchor) and **4** (pyridyl anchor) are red-shifted by ca. 40 nm compared with **3** (hydroxyl anchor), which has the most blue-shifted absorption peak (Table 1). Employing the sulfonate anchor leads to

Table 1. Absorptivity and Peak Absorption Wavelengths of 1−4 from Experimental UV/Vis Absorption Spectroscopy and TDDFT Calculations in Vacuo and in DMSO Solution

	ε ($\times 10^3$ M^{-1} cm^{-1})			λ_{max} (nm)		
dye	exp.[a]	calcd[b]	calcd[c]	exp.[a]	calcd[b]	calcd[c]
1	29	48	51	448	456	456
2	31	48	51	430	451	452
3	48	46	48	415	426	427
4	42	44	46	462	434	434

[a]Experimentally determined UV/vis absorption spectra. [b]TDDFT calculations in vacuo. [c]TDDFT calculations in DMSO solution.

moderate light harvesting prospects of **2**, in terms of peak absorption wavelength among the subject dyes, where red-shifting to the near IR region is ideal for DSSC performance. **3** exhibits a shoulder, centered at ca. 450 nm, on the main absorption peak at 415 nm; this shoulder is probably due to the hydrazone tautomer, this being common in the hydroxyl azo dye compounds.[62] Overall, the light absorbing peak wavelengths in DMSO follow the ranking **4** > **1** > **2** > **3**, and the ranking is the same for the light absorption peak wavelengths in ethanol solvent (see Figure S1 in the Supporting Information). This ranking of UV/vis peak absorption wavelength is consistent with the relative ordering of the Hammett values of the substituted anchor group in these dyes;[63] the hydroxyl group has a undesirable negative $\sigma_p - \sigma_m$ value[64] and thus acts as an electron donor, thereby requiring more energy to induce the $\pi\cdots\pi^*$ transition.

Solvatochromism effects of **1** were also investigated (see Figure S2 in the Supporting Information) and a bathochromic shift was observed when the solvent becomes more polar, e.g. a solvent such as DMSO. **3** exhibited the largest light absorptivity ($\approx 48 \times 10^3$ M^{-1} cm^{-1}) although its light absorbing wavelength is inferior. The absorptivity of **1** was found to be slightly lower than the same observed in a previous study,[33] probably because of its inherent solubility issues because some precipitates existed in various solvents at low concentration after prolonged heating and stirring. Fluorescence spectroscopy was also attempted for **1**−**4** in DMSO, but little emission exists, indicating that the dominant relaxation of molecules from excited state to ground state is nonradiative when in a polar solvent.

Complementary TDDFT simulations (Figure 1b, c) predict well the experimentally determined UV/vis absorption spectra of the four dyes with the peak absorption wavelengths of all dyes being centered at ca. 450 nm; the hydroxyl anchor presenting the most blue-shifted absorption spectra for **3**; **2** showing a slight blue-shift compared with **1**. Two bands are observed in the UV/vis absorption region for all the dyes, one at ca. 300 nm and the other one near the aforementioned 450 nm. Solvent inclusion in the TDDFT calculations has a negligible effect on the peak wavelength, whereas obvious changes in absorptivity are apparent: solvent inclusion universally increases the calculated absorptivity at the peak wavelength (Table 1). This is probably due to the solvent effects on the orbitals overlap. The absorptivity is affected by the overlap between the occupied and unoccupied orbitals. On the other hand, peak wavelength is less prone to orbital overlap; thus, the peak position remains invariant using the implicit solvent model in this study.

The red-shift observed in experimental absorption spectra for **4** is not replicated by calculations. Two mechanisms are proposed to be responsible for this experimentally observed solution-based phenomenon in **4**. Firstly, J-aggregation exists for **4**. Secondly, trans to cis photoisomerization might also exist for **4**. Both of these two mechanisms could cause severe red shifts in the UV/vis absorption spectra of dyes in solution.[65,66]

Electrochemical Trends in 1−4. Cyclic voltammetry (CV) is an effective tool to determine the molecular energy levels of dyes, which is crucial for considering their abilities in

terms of electron injection into the TiO_2 semiconductor oxide and dye regeneration from the electrolyte. In Figure 2, **3** shows

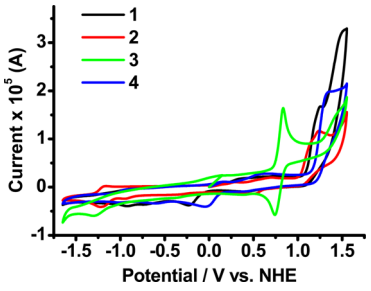

Figure 2. Cyclic voltammetry curves of **1**−**4** in DMSO solution. The HOMO energy level could be approximated by the center of the anodic and cathodic peak potentials.

a reversible redox process corresponding to oxidation at 0.79 V versus the normal hydrogen electrode (NHE), whereas **1**, **2**, and **4** exhibit quasi-reversible waves and their oxidation peaks are estimated to be 1.13, 1.14, and 1.21 V versus NHE, respectively.

Table 2 demonstrates that the molecular energy levels of the frontier orbitals given by DFT calculations agree qualitatively with CV results; the hydroxyl anchor has the lowest HOMO level versus NHE while the other three anchors present similar values. The DMSO solvent inclusion in the calculation shifts the HOMO energy upwards versus NHE (i.e., shifts the HOMO energy level downwards versus the vacuum level), except for the case of the sulfonate anchor.

The band gap ($E_{0\text{-}0}$) values estimated by the UV/vis absorption onset from experimental data (Table 2) show that the use of the carboxylate anchor leads to the most desirable (smallest) band gap for **1**, whereas the use of the hydroxyl anchor, in **3**, exhibits the largest band gap. The $E_{0\text{-}0}$ values estimated via both DFT and TD-DFT in vacuo and when in DMSO solution (Table 2) agree with this experimentally observed trend. Solvent inclusion in the DFT calculations affords a reduction in the band gap, rendering it closer to the experimentally determined values. When the TDDFT calculated first excitation energy is used to approximate the band gap, the value is even more agreeable with experiment. An underestimation of the band gap by DFT that is frequently encountered when modelling solid media does not occur in the cluster model (Table 2). Progressing from small cluster (cluster model) to condensed matter (slab model), a greater density of states is introduced; as a result, the band splits and widens. This is equivalent to saying that the band gap in the cluster model, defined by the difference between LUMO and HOMO, is much larger than the E_g defined by the difference between CBM and VBM in the slab model.

Regarding the LUMO energy levels, **1** and **4** have similar values versus NHE, whereas **3** has consistently the smallest value versus NHE. The LUMO energy levels follow the same trend as the $E_{0\text{-}0}$ values, and those estimated by TDDFT first excitation energies, where embracing the solvent effects improves the computational accuracy compared with experimental results (Table 2).

Frontier Molecular Orbital Considerations for 1−4. To visualize the relative molecular energy levels in a more direct DSSC context, the values of calculated HOMO−1 (H-1), HOMO (H), LUMO (L) and LUMO+1 (L) energy levels versus vacuum for both the free dyes and the dye/TiO_2 nanocomposites of **1**−**4** are plotted with reference to the edge of the TiO_2 conduction band and the I^-/I_3^- redox couple energy level (Figure 3). All of the LUMO energy levels of the dye/TiO_2 nanocomposites are high enough to enable electron injection into the TiO_2 conduction band edge, whereas their HOMO energy levels are low enough to be regenerated by the electrolyte.

Figure 4 also permits a ready assessment of the energetic effects of dye anchoring onto the TiO_2. The energy levels of LUMO and LUMO+1 of the free dyes are lower than those of the combined dye/TiO_2 system, because of the additional states introduced by TiO_2. Moreover, neighboring energy levels in the dye/TiO_2 system are much closer than those of the free dyes; this is expected, since more electronic states are introduced by the semiconductor oxide surface. **3**/TiO_2 has the highest LUMO energy level, indicating an excess of energy upon excitation, leading to wasted energy expenditure through thermal relaxation and a lower extent of dye regeneration from the electrolyte.

The corresponding molecular orbital distributions offer an intuitive view about charge separation: the "push−pull" effect is strengthened if further separation between the occupied orbital and unoccupied orbital distributions is realized.[67,68] HOMO−1, HOMO, LUMO, and LUMO+1 have been shown to be the salient orbital distributions that are important for these azo dyes[65] and dye/TiO_2 combined system, and so particular attention is given to them, c.f. their presentation in Figure 4 for each dye attached to TiO_2. This shows that the carboxylate, sulfonate, and pyridyl anchors offer similar HOMO and LUMO distributions: the HOMOs are mainly localized in the donor region of the organic dyes, whereas the LUMOs lie mainly in the TiO_2 cluster, which is an indicator of a large driving force for charge separation;[33] on the contrary, **3**/TiO_2 presents HOMOs that are delocalized throughout the organic molecule. The primary orbital contribution to the HOMO−1 for all four

Table 2. HOMO and LUMO Energy Levels, As Well as $E_{0\text{-}0}$ (band gap) Values (versus NHE), Taken from Experimental Data and DFT/TDDFT Calculations

	HOMO (V) (versus NHE)			$E_{0\text{-}0}$ (eV)					LUMO (V) (versus NHE)				
dye	exp[a]	calcd[d]	calcd[e]	exp[b]	calcd[d]	calcd[e]	calcd[f]	calcd[g]	exp[c]	calcd[d]	calcd[e]	calcd[f]	calcd[g]
1	1.13	0.86	0.88	2.16	3.14	2.90	2.56	2.54	−1.03	−2.28	−2.02	−1.70	−1.65
2	1.14	1.03	0.95	2.28	3.15	2.91	2.57	2.54	−1.14	−2.11	−1.96	−1.54	−1.59
3	0.79	0.48	0.64	2.34	3.33	3.14	2.77	2.75	−1.55	−2.85	−2.50	−2.29	−2.11
4	1.21	0.88	0.91	2.16	3.25	3.00	2.61	2.58	−0.95	−2.37	−2.09	−1.73	−1.67

[a]Cyclic voltammetry (CV). [b]The UV/vis absorption edge. [c]The difference between HOMO energy levels determined via CV and $E_{0\text{-}0}$ from the UV/vis absorption edge. [d]DFT calculations in vacuo. [e]DFT calculations in DMSO solution. [f]The first excitation energy via TDDFT calculations in vacuo. [g]The first excitation energy via TDDFT calculations in DMSO solution.

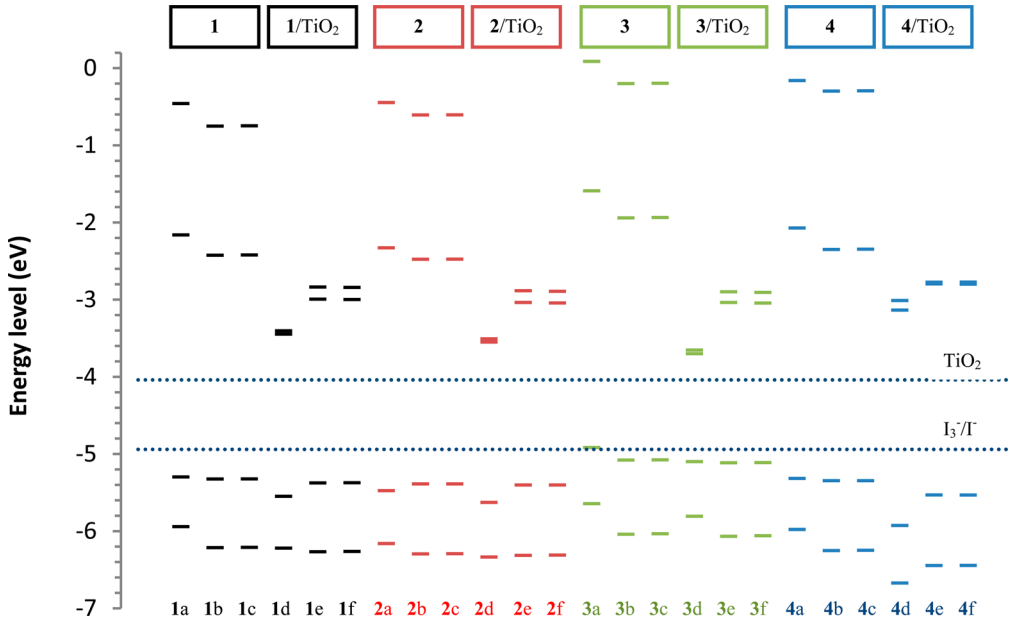

Figure 3. Energy levels (from top to down: L+1, L, H, and H-1) of **1**−**4** from DFT calculations. a−c correspond to the free dye calculations (a, in vacuo; b, DMSO; c, acetonitrile), whereas d−f are their corresponding dyes/TiO_2 system (d, dye/TiO_2 in vacuo; e, dye/TiO_2 in DMSO; f, dye/TiO_2 in acetonitrile). TiO_2 (−4.04 eV) and I_3^-/I^- (−4.94 eV) energy levels from literature[69] are also shown.

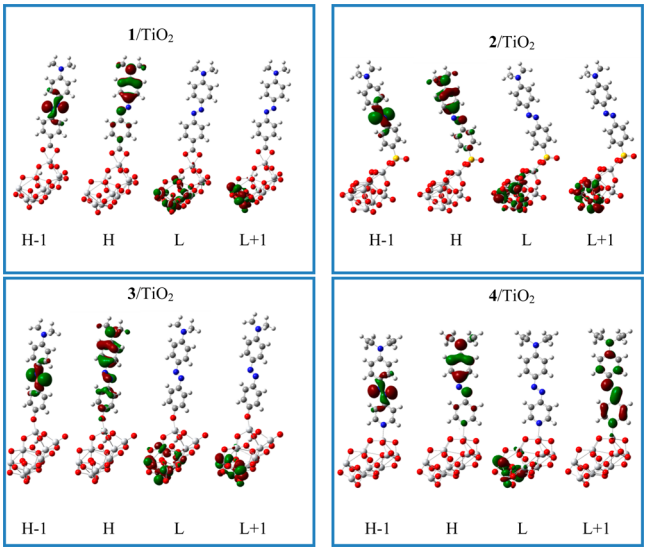

Figure 4. Orbital distributions of HOMO-1 (H-1), HOMO (H), LUMO (L), and LUMO+1 (L+1) of the dye/TiO_2 systems optimized in vacuo.

azo dyes resides in the azo group, which is a typical characteristic for these azo dyes.[65] With the stark exception of **4**/TiO_2, the LUMO+1 level distributions of the **1**/TiO_2-**3**/TiO_2 reside in the TiO_2 cluster. In **4**/TiO_2, the LUMO+1 is anomalously distributed within the dye region and in a fashion that is not ideal for charge transfer purposes. Bearing in mind all of these HOMO−1, HOMO, LUMO, and LUMO+1 orbital distribution characteristics, the extent of charge separation in these four dyes presumably follow the ranking **1** > **2** > **4** > **3**, on the basis of these isolated dye/TiO_2 cluster calculations.

Isolated Cluster Versus Periodic 2D Structure Calculations. With a bidentate bridging anchoring mode for the carboxylate and sulfonate groups, and a direct coupling between the anchor and the surface unsaturated titanium atom for the pyridyl and hydroxyl groups, dye/TiO_2 structures were optimized successfully using plane-wave basis sets (Figure 5).

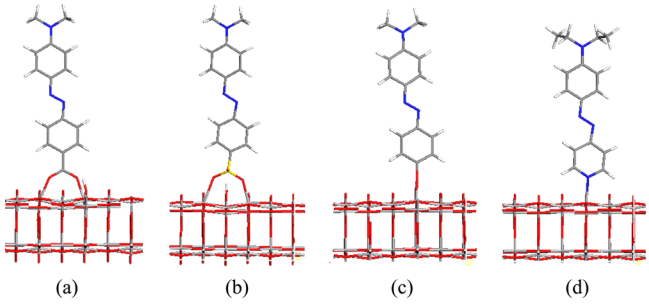

Figure 5. Optimized structures of (a) **1**/TiO_2, (b) **2**/TiO_2, (c) **3**/TiO_2, and (d) **4**/TiO_2 in a unit cell from the plane wave calculations (Method 2), visualized via Mercury.[70] Red, oxygen; blue, nitrogen; dark grey, carbon; light grey, titanium. White: hydrogen. Yellow: sulfur.

The intermolecular distance, which dictates the extent of dye coverage, is controlled by the size of the unit cell (see Figures S3 and S4 in the Supporting Information); a model where each dye molecule repeats every other 11.4 Å × 10.5 Å units in the 2D structure was calculated.

The HOMO and conduction band minima (CBM) of the dye/TiO_2 system at the Γ-point, revealed by Method 2 (Figure 6), are similar to those of HOMOs and LUMOs from Method 1. HOMOs of the combined system are localized in the region near the donor of these dyes, except for **3**/TiO_2 which displays "diffusion" to the coupling site at the hydroxyl group/TiO_2 interface. The distributions of CBM and CBM+1 are both localized in the TiO_2 moiety, showing Ti(3d) orbital characteristics; this is ideal for the "push-pull" effect that benefits charge injection. The CBM+1 surface for **4**/TiO_2, identical with the prediction from Method 1, appears slightly "protruded" towards the HOMO region, which stands to diminish donor−acceptor separations and the "push−pull"

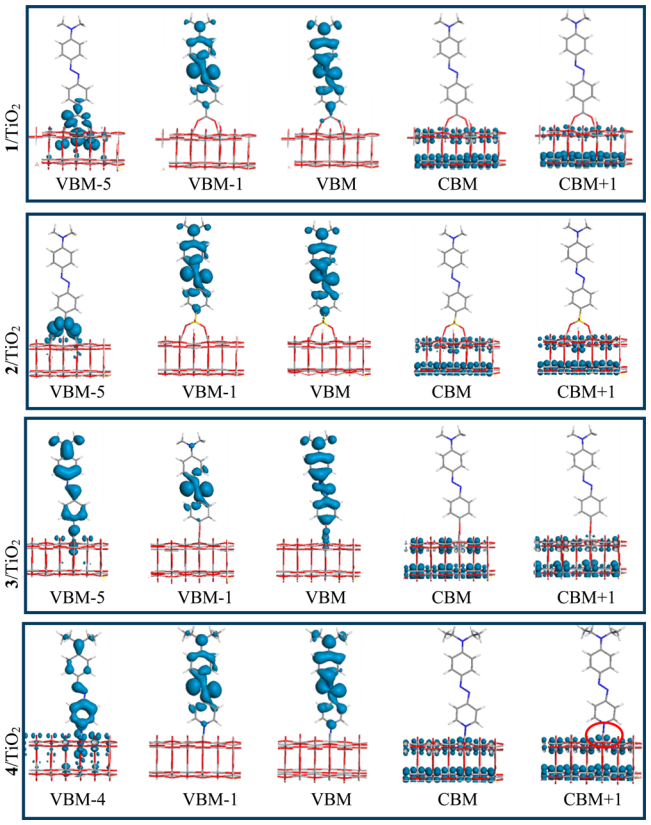

Figure 6. Orbital distributions of VBM-1, VBM, CBM, and CBM+1 of the four dyes with different anchors; that of VBM-5 is also shown for **1**/TiO_2-**3**/TiO_2, whereas **4**/TiO_2 displays orbital distributions in VBM-4.

strength of intramolecular charge transfer in the dye. The VBM-1 distributions are predominantly localized within the azo group for **1**/TiO_2–**4**/TiO_2, similar to the case of HOMO−1 distributions, obtained from Method 1 (Figure 3). In addition, the distributions of VBM-5 for **1**/TiO_2-**3**/TiO_2 and VBM-4 for **4**/TiO_2 (Figure 6, left) are located at the dye/TiO_2 interface, indicating strong coupling between the organic dye and the inorganic semiconductor counterpart. The CBM distributions reside mainly in Ti(3d) orbitals, while those of VBM and VBM-1 lie principally in the π-conjugated bonding and the azo group. In summary, the "push–pull" charge-transfer effects inferred by these orbital distributions follow the ranking **1** > **2** > **4** > **3**, on the basis of the combined model of a dye located on the surface of a 2D periodic slab of TiO_2.

The band gaps determined by Method 2 are 2.545 eV for the pure TiO_2 slab, 0.803 eV for **1**/TiO_2, 0.461 eV for **2**/TiO_2, 0.396 eV for **3**/TiO_2, and 1.227 eV for **4**/TiO_2, which means that the dye/TiO_2 composite system is still a semiconductor. Interestingly, both Method 1 and Method 2 predict **3**/TiO_2 to have the smallest band gap, although **3** is deficient in light absorption in its free dye form, as evidenced both experimentally and computationally, c.f. Figure 1. This might partly explain the optimal functionality of the salicyclic anchor in a DSSC, which features both a hydroxyl and carboxylate group.[71]

Inferring Dye/TiO_2 Interface from UV/vis Absorption Spectra. One can infer the dye/TiO_2 interface and dye loading by studying the time evolution of UV/vis absorption spectra in dye/TiO_2 films (Figure 7). After a 15 min-sensitization in a

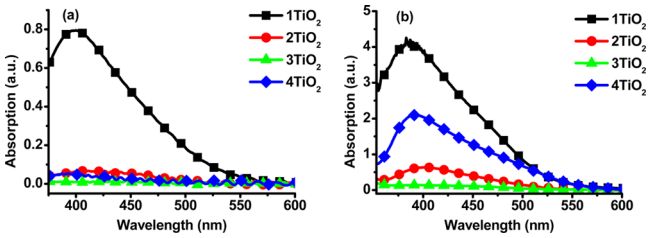

Figure 7. (a) UV/vis absorption spectra of the dye/TiO_2 films sensitized in 0.05 mM 1:1 acetonitrile/tert-butanol for 15 min. (b) UV/vis absorption spectra of the films sensitized in 0.5 mM 1:1 acetonitrile/tert-butanol for 24 h. The films were carefully rinsed with ethanol to remove the excess unadsorbed dyes.

diluted 0.05 mM 1:1 acetonitrile/tert-butanol solution (Figure 7a), a film of **1**/TiO_2 exhibited an absorption intensity of ca. 0.8 a.u. at peak absorption wavelength, whereas the films of **2** and **4** displayed much less (ca. 0.1 a.u.) light absorption, and thus a lower extent of dye loading, considering the absorptivity of free dyes (Figure 1). After prolonged sensitization for ca. 24 h in a 0.5 mM 1:1 acetonitrile/tert-butanol solution, the differences caused by sulfonate, hydroxyl and pyridyl anchors are more obvious (Figure 7b). The pyridyl group bearing dye, **4**, presents a significant level of adsorption onto TiO_2, as demonstrated by its intense absorption intensity of ∼2 a.u.. The dye with the sulfonate anchor (**2**) shows a moderate performance (ca. 0.5 a.u. absorption intensity), whereas the dye containing the hydroxyl group (**3**) displays the poorest light absorption. The inherent light harvesting abilities of the films of **1**–**4** therefore follow the ranking **1** > **4** > **2** > **3**.

H-aggregation is present in all of the dyes on TiO_2 films, as is evidenced by the 20–50 nm blue-shifting of their UV/vis peak absorption wavelengths, compared with those of solution-based measurements on the free dyes (Figure 1a).

When the adsorption bath is changed from 1:1 acetontrile/tert-butanol to DMSO, the films yield much less UV/vis absorption except for **1** (Figure 8). Amongst all of the anchors,

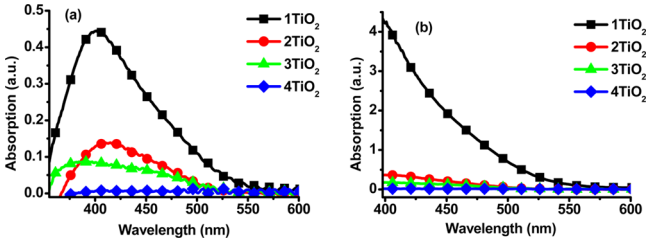

Figure 8. (a) UV/vis absorption spectra of **1**, **2**, **3**, and **4** on TiO_2 films, having been immersed in 0.05 mM DMSO solution for ca. 15 min. After rinsing, **4** shows almost no absorption, indicating poor adsorption strength of the pyridyl anchoring group in DMSO solution. (b) UV/vis absorption of **1**, **2**, **3**, and **4** on TiO_2 films, having been immersed in 0.5 mM DMSO solution for 24 h. DMSO induces H aggregation; the region below 400 nm exceeds the accurate detector region; as a result, only ca. 400 nm to 600 nm are shown.

the pyridyl group is by far the most vulnerable to different adsorption baths: after prolonged adsorption time of ca. 24 h, the corresponding **4**/TiO_2 film obtained by sensitization in DMSO exhibits negligible light absorption, while the one sensitized in 1:1 acetonitrile/tert-butanol displayed significant light absorption, peaking at ∼2 a.u.. The light harvesting underperformance of **4**/TiO_2 sensitized in DMSO solution is

dx.doi.org/10.1021/am502186k | ACS Appl. Mater. Interfaces 2014, 6, 7535–7546

possibly due to the competing nucleophilic capability of DMSO and pyridine onto the five-fold titanium site.

Compared with the calculated UV/vis absorption spectra of the free dyes (Figure 1b), the TDDFT calculation on the dye/TiO_2 systems based on the Method 1 generally predicts a blue-shift of UV/vis absorption spectra, especially for **2**. This agrees with the trend observed from experiments (Figures 1a and 7b), where the light absorption peak is blue-shifted to ca. 400 nm for the dye/TiO_2 film (Figure 7b). The only exception is **3**, which has a red-shifted UV/vis absorption spectra upon sensitization on TiO_2 substrate. Interestingly, its absorptivity at peak absorption wavelength diminished in the dye/TiO_2 composite, which is subtly captured by Method 2 (Figure 9b). Both

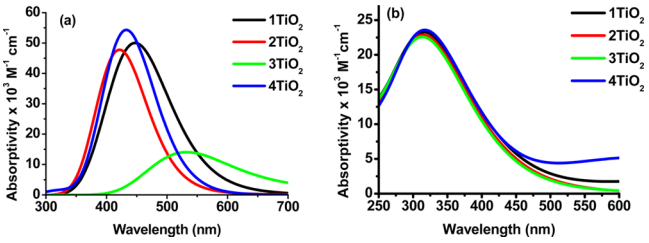

Figure 9. (a) UV/vis absorption spectra of (**1**–**4**)/TiO_2 from TDDFT calculations in vacuo. (b) Optical absorption of (**1**–**4**)/TiO_2 based on the dielectric constant calculations employed via Method 2.

methods partly explain the negligible light absorption of the film sensitized by **4**. Overall, the optical properties of the dye/TiO_2 combined system predicted by Method 1 are more sensitive to different anchors than those by Method 2; this is probably due to a larger dye contribution to the whole system in Method 1, judging by its similar numbers of atoms of the dye and the TiO_2 cluster.

Larger adsorption energies show greater ability to immobilize the dyes on the TiO_2 surface and promote dye-TiO_2 coupling.[72] From DFT calculations (Table 3), the dye/TiO_2 adsorption energies calculated in acetonitrile from Method 1 are slightly larger than those in DMSO; these findings agree with experiment. Both methods predict that the sulfonate anchor leads to the largest adsorption energy, followed by the pyridine anchor. The carboxylic acid and hydroxyl anchors exhibit similar values. Overall, the adsorption energies predicted by Method 1 are universally larger than those from Method 2 (by 0.1–0.4 eV), probably because of the more reactive nature of a small nanocluster "reactant" compared with a large periodic slab.

After desorption of the dye from the TiO_2 nanocomposite films, using aqueous sodium hydroxide, the UV/vis absorption spectra of the resulting dye solutions were measured so that the dye loading in each film could be inferred (Table 3). The carboxylate anchor leads to **1** demonstrating the largest dye loading onto the TiO_2 semiconductor, while the hydroxyl anchor leads to the smallest. Table 3 shows that the dye loading experimentally determined follows the ranking, **1** > **4** > **3** > **2**. The dye loading calculated via Method 2, which is controlled by the size of unit cell constructed, is listed as a reference, although it renders a poor estimate. The significant under-estimation of dye coverage employed in the model is most likely due to the following two reasons: firstly, a flat 2D monolayer surface is constructed in the model, but in reality the particles are spherical-like and surrounded by dye molecules in all directions. Secondly, dimer, trimer and higher-order aggregates that are also present in reality cause an additional level of dye adsorption. It has been demonstrated that such aggregation (either J- or H-type) is common for dyes adsorbed onto TiO_2, unless a co-adsorbent such as deoxycholic acid (DCA) is included for anti-aggregation purposes.[18,73−82] For these azo dyes specifically, H-aggregation dominates, as evidenced earlier by UV/vis absorption spectra which are blue-shifted in the dye/TiO_2 film relative to dyes in solution (Figure 1 versus Figures 7 and 8).

Dye/TiO_2 Embedded DSSC Device Characteristics. The external quantum efficiency (EQE) peak intensity of DSSCs containing the dye/TiO_2 nanocomposites as their working electrodes follows the ranking, **1** > **2** > **4** > **3**. **1** is superior in its associated DSSC performance conversion efficiency (Table 3) and accounts for 8% of the N3 performance employing the same fabrication and testing conditions, whereas **2**–**4** present 1.2 to 2% of that from N3. Multi-duplicate cell fabrication and testing enabled good consistency checking in their DSSC performance (see Table S1 in the Supporting Information), the results of which suggest an overall device efficiency ranking of **1** > **4** > **2** > **3**. The detailed EQE spectral response and photovoltaic $J-V$ curves of each DSSC (Figure 10) unambiguously indicate that devices containing **1** exhibit the best device performance, **3** the worst, with **2** and **4** presenting as moderate EQE. This is consistent with the aforementioned salient electronic and optical findings of this work.

Experimentally, the carboxylic acid anchor exhibits the largest conversion efficiency among the four anchors, which explains the majority of research based on the carboxylic acid anchor. In stark contrast, the hydroxyl group anchor exhibits negligible light absorption and conversion efficiency of the sensitized film,

Table 3. Adsorption Energies Calculated Using a Localized Basis Set (in vacuo, in DMSO, and in acetonitrile solvent); Adsorption Energies and Dye Coverage Estimates Obtained from Plane-Wave Calculations; External Quantum Efficiency (EQE), Overall Performance Conversion Efficiency of the Dyes in DSSC Devices (η), and the Efficiency Referenced with N3 Performance (η_{dye}/η_{N3})

dye	adsorption energy calcd (in vacuo) (eV).[a]	adsorption energy calcd (DMSO) (eV)[b]	adsorption energy (MeCN) calcd (eV)[c]	adsorption energy (periodic) (eV) calcd[d]	dye loading (nmol/cm^2) exp[e]	dye loading (nmol/cm^2) calcd[f]	peak EQE exp. (%)	η exp. (%)	η_{dye}/η_{N3} exp. (%)
1	1.64	0.88	0.89	0.52	147	0.14	22	0.20	8
2	1.77	1.06	1.06	0.94	66	0.14	11	0.04	1.6
3	1.51	0.80	0.81	0.53	28	0.14	2	0.03	1.2
4	1.65	1.04	1.05	0.82	93	0.14	3	0.05	2

[a]Method **1** in vacuo. [b]Method **1** in DMSO. [c]Method **1** in acetonitrile. [d]Method **2**. [e]from NaOH desorption experiment. [f]from Method **2**.

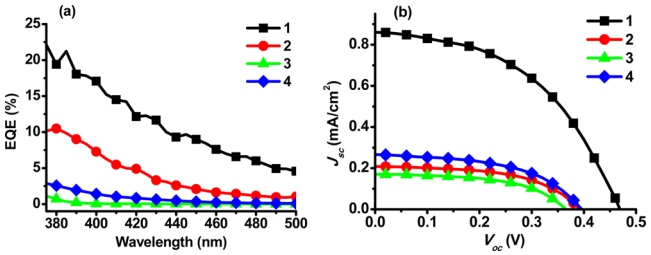

Figure 10. (a) EQE spectra of **1**–**4** embedded into DSSCs, which present a ranking, **1** > **2** > **4** > **3** (for reference N3 dye-embedded DSSC yields an internal EQE peak value of ca. 65%). (b) Typical *J*–*V* curves of DSSCs of **1**–**4**. DSSCs containing the reference N3 dye exhibit 2.5% efficiency when fashioned under at the same device fabrication and testing conditions as per **1**–**4**.

which contradicts findings in the existing literature.[83] To reconcile this ostensible inconsistency, we propose that the hydroxyl group actually acts as an "auxiliary anchor", which is applicable in DSSC dyes only when these molecules also possess other functional groups, such as the case for catechol, 8-hydroxylquinoline and 2-hydroxylquinoline;[84−86] when the hydroxyl groups are used in the absence of such functional moieties, the DSSC performance is insufficient due to negligible dye adsorption. The sensitization of dyes on a TiO_2 substrate with sulfonate and pyridyl groups is evident, and is compatible with previous results.[87−95] Nevertheless, these two groups, although exhibiting obvious sensitization, offer much lower photovoltaic effects than those of the carboxylic acid anchor. Computationally, the carboxylic acid anchor leads to a bidentate anchoring mode, which is compatible with the majority of previous research findings. There remains a dearth of theoretical understanding about possible adsorption modes for sulfonate, hydroxyl, and pyridyl anchors; accordingly, this study has identified stable dissociative adsorption modes by these anchors and the unsaturated surface titanium atoms. The hydroxyl group exhibits insufficient light absorption theoretically (Figure 9), which partly explains its inferiority as an anchor for DSSC dyes.

CONCLUSIONS

The four dye···semiconductor anchors, carboxylate, sulfonate, hydroxyl, and pyridyl, presented in this study reveal distinctive differences in their light absorption spectra, molecular orbital energy levels, molecular orbital distribution, band gaps, amount of dye adsorption and overall conversion efficiency. The anchors are sensitive to the sensitization solvent, especially for pyridyl groups, where the corresponding dye exhibits negligible amounts of adsorption in DMSO solvent.

The pyridyl-containing dye, **4**, displays the greatest red-shift in UV/vis peak absorption wavelength and the most desirable level of adsorption when a suitable sensitization solvent is chosen. In contrast, the charge-transfer "push−pull" attributes of **4** are not optimal when the dye is anchored onto the TiO_2 semiconductor; this is manifested in its lower EQE and DSSC performance conversion efficiency, compared with **1** that bears a carboxylate anchor. The sulfonate-containing dye, **2**, exhibits similar electronic and optical properties as **4**. The dye featuring a hydroxyl anchor, **3**, yields the worst performance, with it inferior UV/vis absorption intensity on TiO_2 substrate and the lowest DSSC performance conversion efficiency.

The carboxylate anchor unquestionably outperforms the other anchors employed in this study, manifest by **1** showing the largest peak EQE and best overall DSSC performance conversion efficiency. Its UV/vis absorptivity also displays a decent level of light absorption, although its light absorption and calculated adsorption energies are not stunning. Detailed calculations on various types of TiO_2 adsorption modes of **1** indicate that the bidentate bridging anchoring mode with hydrogen dissociated to the TiO_2 surface is the most stable mode, among seven possible configurations.

Overall, this study serves to find ways of making the family of azo dyes function better in DSSCs, given the prospects of azo dyes due to availability and cost-effectiveness. It has been confirmed that the functionality of the azo dyes strongly depend on different anchors. All of the azo dyes exhibit H-aggregation when anchored onto TiO_2 semiconductor, suggesting that none of their associated anchors are sufficiently strong enough to affect the intermolecular interactions of the dye monolayer on the TiO_2 semiconductor.

The predictions of electronic and optical properties, based on either an isolated dye/TiO_2 cluster or a dye modeled on the surface of a 2D periodic structure, agree well with each other in many ways; together they offer a comprehensive view on the structure-property relationships ensuing at the dye···semiconductor interface. Both cluster and slab models predict the bidentate adsorption mode to be stable, and suggest non-desirable optical absorption of the hydroxyl anchor. Orbital distributions indicate that the highest occupied energy levels have contributions primarily emanating from orbitals of the dye, whereas the CBM is dominated by contributions from Ti 3d orbitals. Push−pull effect exists, although these are not strong because of the slight delocalization of the VBM (HOMO) orbital in the molecule. The slab model allows a convenient way to predict the dye coverage due to the well-defined unit cell, although it is somewhat primitive and lacks solvent effects. Improvements in modelling the coverage prediction can be achieved by modifying the size of a unit cell in the slab model. From the experimental UV/vis absorption spectra of the sensitized film, dye coverage seems to be critical to the overall conversion efficiency. Further study on the dye coverage and aggregation effects on the anatase surface, based on these two models, would be beneficial.

The overall conversion efficiencies of these azo dyes are not large, which probably originates from undesired aggregation and halogen-bond formation between azo groups and the electrolyte. However, this issue can be circumvented by realizing improvements in the synthetic route to these dyes, such as the judicious introduction of certain side groups and bulky donors onto the parent dye molecules. In more general terms, this study also serves as an exemplar for further efforts to model interfaces in DSSCs. Detailed comparison studies of such calculated models, as presented here, are particularly important given that there remains a distinct dearth of suitably advanced experimental materials characterization tools that can probe buried interfaces in a non-destructive manner and in an operational device.

ASSOCIATED CONTENT

Supporting Information

Consistency checklist of DSSC performances of **1**–**4**; seven different possible adsorption modes for **1**; adsorption energies of **1** with different types of carboxylate···TiO_2 anchoring modes; normalized absorption spectra of **1**, **2**, **3** and **4** in ethanol; solvatochromism of **1**; side view of 1 × 3 × 1 supercell of optimized structure of **1** on TiO_2; and top view of the 6 × 6

× 1 supercell of **1** on TiO_2 are deposited in the Supporting Information. This material is available free of charge via the Internet at http://pubs.acs.org.

AUTHOR INFORMATION

Corresponding Author

*E-mail: jmc61@cam.ac.uk. Tel: +44 (0)1223 337470. Fax: +44 (0)1223 373536.

Author Contributions

The manuscript was written through contributions of all authors. All authors have given approval to the final version of the manuscript.

Notes

The authors declare no competing financial interest.

ACKNOWLEDGMENTS

J.M.C. thanks the Fulbright Commission for a UK-US Fulbright Scholar Award, hosted by Argonne National Laboratory, where work done was supported by the DOE Office of Science, Office of Basic Energy Sciences, under Contract DE-AC02-06CH11357. The authors acknowledge support from the EPSRC UK National Service for Computational Chemistry Software (NSCCS), and the Cambridge High Performance Computing Cluster (HPC, Darwin).

REFERENCES

(1) Hardin, B. E.; Snaith, H. J.; McGehee, M. D. The Renaissance of Dye-Sensitized Solar Cells. *Nat. Photonics* **2012**, *6*, 162−169.

(2) Grätzel, M. Photoelectrochemical Cells. *Nature* **2001**, *414*, 338−344.

(3) Zou, W.; Visser, C.; Maduro, J. A.; Pshenichnikov, M. S.; Hummelen, J. C. Broadband Dye-Sensitized Upconversion of near-Infrared Light. *Nat. Photonics* **2012**, *6*, 560−564.

(4) O'Regan, B.; Grätzel, M. A Low-Cost, High-Efficiency Solar Cell Based on Dye-Sensitized Colloidal TiO_2 Films. *Nature* **1991**, *353*, 737−740.

(5) Xie, Z.; Jin, X.; Chen, G.; Xu, J.; Chen, D.; Shen, G. Integrated Smart Electrochromic Windows for Energy Saving and Storage Applications. *Chem. Commun.* **2014**, *50*, 608−610.

(6) Bechinger, C.; Ferrere, S.; Zaban, A.; Sprague, J.; Gregg, B. A. Photoelectrochromic Windows and Displays. *Nature* **1996**, *383*, 608−610.

(7) Ahn, K.-S.; Yoo, S. J.; Kang, M.-S.; Lee, J.-W.; Sung, Y.-E. Tandem Dye-Sensitized Solar Cell-Powered Electrochromic Devices for the Photovoltaic-Powered Smart Window. *J. Power Sources* **2007**, *168*, 533−536.

(8) Hardin, B. E.; Hoke, E. T.; Armstrong, P. B.; Yum, J.-H.; Comte, P.; Torres, T.; Fréchet, J. M. J.; Nazeeruddin, M. K.; Grätzel, M.; McGehee, M. D. Increased Light Harvesting in Dye-Sensitized Solar Cells with Energy Relay Dyes. *Nat. Photonics* **2009**, *3*, 406−411.

(9) Anthonysamy, A.; Lee, Y.; Karunagaran, B.; Ganapathy, V.; Rhee, S.-W.; Karthikeyan, S.; Kim, K. S.; Ko, M. J.; Park, N.-G.; Ju, M.-J.; et al. Molecular Design and Synthesis of ruthenium(II) Sensitizers for Highly Efficient Dye-Sensitized Solar Cells. *J. Mater. Chem.* **2011**, *21*, 12389−12397.

(10) Chen, K.-S.; Liu, W.-H.; Wang, Y.-H.; Lai, C.-H.; Chou, P.-T.; Lee, G.-H.; Chen, K.; Chen, H.-Y.; Chi, Y.; Tung, F.-C. New Family of Ruthenium-Dye-Sensitized Nanocrystalline TiO_2 Solar Cells with a High Solar-Energy-Conversion Efficiency. *Adv. Funct. Mater.* **2007**, *17*, 2964−2974.

(11) Clifford, J. N.; Palomares, E.; Nazeeruddin, M. K.; Grätzel, M.; Nelson, J.; Li, X.; Long, N. J.; Durrant, J. R. Molecular Control of Recombination Dynamics in Dye-Sensitized Nanocrystalline TiO_2 Films: Free Energy vs Distance Dependence. *J. Am. Chem. Soc.* **2004**, *126*, 5225−5233.

(12) Nazeeruddin, M. K.; Péchy, P.; Renouard, T.; Zakeeruddin, S. M.; Humphry-Baker, R.; Comte, P.; Liska, P.; Cevey, L.; Costa, E.; Shklover, V.; et al. Engineering of Efficient Panchromatic Sensitizers for Nanocrystalline TiO_2-Based Solar Cells. *J. Am. Chem. Soc.* **2001**, *123*, 1613−1624.

(13) Burschka, J.; Pellet, N.; Moon, S.-J.; Humphry-Baker, R.; Gao, P.; Nazeeruddin, M. K.; Grätzel, M. Sequential Deposition as a Route to High-Performance Perovskite-Sensitized Solar Cells. *Nature* **2013**, *499*, 316−319.

(14) Alibabaei, L.; Kim, J.-H.; Wang, M.; Pootrakulchote, N.; Teuscher, J.; Di Censo, D.; Humphry-Baker, R.; Moser, J.-E.; Yu, Y.-J.; Kay, K.-Y.; et al. Molecular Design of Metal-Free D−π−A Substituted Sensitizers for Dye-Sensitized Solar Cells. *Energy Environ. Sci.* **2010**, *3*, 1757.

(15) Fischer, M. K. R.; Wenger, S.; Wang, M.; Mishra, A.; Zakeeruddin, S. M.; Grätzel, M.; Bäuerle, P. D-Π-A Sensitizers for Dye-Sensitized Solar Cells: Linear vs Branched Oligothiophenes. *Chem. Mater.* **2010**, *22*, 1836−1845.

(16) Clifford, J. N.; Martínez-Ferrero, E.; Viterisi, A.; Palomares, E. Sensitizer Molecular Structure-Device Efficiency Relationship in Dye Sensitized Solar Cells. *Chem. Soc. Rev.* **2011**, *40*, 1635−1646.

(17) Mishra, A.; Fischer, M. K. R.; Bäuerle, P. Metal-Free Organic Dyes for Dye-Sensitized Solar Cells: From Structure: Property Relationships to Design Rules. *Angew. Chem., Int. Ed.* **2009**, *48*, 2474−2499.

(18) Ooyama, Y.; Inoue, S.; Nagano, T.; Kushimoto, K.; Ohshita, J.; Imae, I.; Komaguchi, K.; Harima, Y. Dye-Sensitized Solar Cells Based on Donor-Acceptor Π-Conjugated Fluorescent Dyes with a Pyridine Ring as an Electron-Withdrawing Anchoring Group. *Angew. Chem., Int. Ed.* **2011**, *123*, 7567−7571.

(19) Brewster, T. P.; Konezny, S. J.; Sheehan, S. W.; Martini, L. A.; Schmuttenmaer, C. A.; Batista, V. S.; Crabtree, R. H. Hydroxamate Anchors for Improved Photoconversion in Dye-Sensitized Solar Cells. *Inorg. Chem.* **2013**, *52*, 6752−6764.

(20) Hirva, P.; Haukka, M. Effect of Different Anchoring Groups on the Adsorption of Photoactive Compounds on the Anatase (101) Surface. *Langmuir* **2010**, *26*, 17075−17081.

(21) Baik, C.; Kim, D.; Kang, M.-S.; Kang, S. O.; Ko, J.; Nazeeruddin, M. K.; Grätzel, M. Organic Dyes with a Novel Anchoring Group for Dye-Sensitized Solar Cell Applications. *J. Photochem. Photobiol., A* **2009**, *201*, 168−174.

(22) Mao, J.; He, N.; Ning, Z.; Zhang, Q.; Guo, F.; Chen, L.; Wu, W.; Hua, J.; Tian, H. Stable Dyes Containing Double Acceptors without COOH as Anchors for Highly Efficient Dye-Sensitized Solar Cells. *Angew. Chem. Int. Ed.* **2012**, *51*, 9873−9876.

(23) Ambrosio, F.; Martsinovich, N.; Troisi, A. What Is the Best Anchoring Group for a Dye in a Dye-Sensitized Solar Cell? *J. Phys. Chem. Lett.* **2012**, *3*, 1531−1535.

(24) Wiberg, J.; Marinado, T.; Hagberg, D. P.; Sun, L.; Hagfeldt, A.; Albinsson, B. Effect of Anchoring Group on Electron Injection and Recombination Dynamics in Organic Dye-Sensitized Solar Cells. *J. Phys. Chem. C* **2009**, *113*, 3881−3886.

(25) Galoppini, E. Linkers for Anchoring Sensitizers to Semiconductor Nanoparticles. *Coord. Chem. Rev.* **2004**, *248*, 1283−1297.

(26) Park, H.; Bae, E.; Lee, J.-J.; Park, J.; Choi, W. Effect of the Anchoring Group in Ru-Bipyridyl Sensitizers on the Photoelectrochemical Behavior of Dye-Sensitized TiO_2 Electrodes: Carboxylate versus Phosphonate Linkages. *J. Phys. Chem. B* **2006**, *110*, 8740−8749.

(27) Bae, E.; Choi, W. Effect of the Anchoring Group (carboxylate vs Phosphonate) in Ru-Complex-Sensitized TiO_2 on Hydrogen Production under Visible Light. *J. Phys. Chem. B* **2006**, *110*, 14792−14799.

(28) Ambrosio, F.; Martsinovich, N.; Troisi, A. Effect of the Anchoring Group on Electron Injection: Theoretical Study of Phosphonated Dyes for Dye-Sensitized Solar Cells. *J. Phys. Chem. C* **2012**, *116*, 2622−2629.

(29) Subramanian, A.; Wang, H.-W. Effect of Hydroxyl Group Attachment on TiO_2 Films for Dye-Sensitized Solar Cells. *Appl. Surf. Sci.* **2012**, *258*, 7833−7838.

(30) Chang, J.-G.; Chen, H.-T.; Ju, S.-P.; Chen, H.-L.; Hwang, C.-C. Role of Hydroxyl Groups in the NH(x) (x = 1-3) Adsorption on the TiO_2 Anatase (101) Surface Determined by a First-Principles Study. *Langmuir* **2010**, *26*, 4813−4821.
(31) Luschtinetz, R.; Frenzel, J.; Milek, T.; Seifert, G. Adsorption of Phosphonic Acid at the TiO_2 Anatase (101) and Rutile (110) Surfaces. *J. Phys. Chem. C* **2009**, *113*, 5730−5740.
(32) Grätzel, M. Recent Advances in Sensitized Mesoscopic Solar Cells. *Acc. Chem. Res.* **2009**, *42*, 1788−1798.
(33) Zhang, L.; Cole, J. M.; Waddell, P. G.; Low, K. S.; Liu, X. Relating Electron Donor and Carboxylic Acid Anchoring Substitution Effects in Azo Dyes to Dye-Sensitized Solar Cell Performance. *ACS Sustain. Chem. Eng.* **2013**, *1*, 1440−1452.
(34) Almeida, M. R.; Stephani, R.; Dos Santos, H. F.; Oliveira, L. F. C. De Spectroscopic and Theoretical Study of the "Azo"-Dye E124 in Condensate Phase: Evidence of a Dominant Hydrazo Form. *J. Phys. Chem. A* **2010**, *114*, 526−534.
(35) Charlton, M. H.; Docherty, R.; McGeein, D. J.; Morley, J. O. Theoretical Investigation of the Structure and Spectra of Donor-Acceptor Azobenzenes. *Faraday Trans.* **1993**, *89*, 1671−1675.
(36) Olmsted, J.; Lawrence, J.; Yee, G. G. Photochemical Storage Potential of Azobenzenes. *Sol. Energy* **1983**, *30*, 271−274.
(37) Jono, R.; Fujisawa, J.; Segawa, H.; Yamashita, K. Theoretical Study of the Surface Complex between TiO 2 and TCNQ Showing Interfacial Charge-Transfer Transitions. *J. Phys. Chem. Lett.* **2011**, *2*, 1167−1170.
(38) Ronca, E.; Pastore, M.; Belpassi, L.; Tarantelli, F.; Angelis, F. De Influence of the Dye Molecular Structure on the TiO_2 Conduction Band in Dye-Sensitized Solar Cells: Disentangling Charge Transfer and Electrostatic Effects. *Energy Environ. Sci.* **2013**, *6*, 183.
(39) Pastore, M.; Angelis, F. De First-Principles Computational Modeling of Fluorescence Resonance Energy Transfer in Co-Sensitized Dye Solar Cells. *J. Phys. Chem. Lett.* **2012**, *3*, 2146−2153.
(40) Pastore, M.; Mosconi, E.; Angelis, F. De Computational Investigation of Dye−Iodine Interactions in Organic Dye-Sensitized Solar Cells. *J. Phys. Chem. C* **2012**, *116*, 5965−5973.
(41) Planells, M.; Pellejà, L.; Clifford, J. N.; Pastore, M.; De Angelis, F.; López, N.; Marder, S. R.; Palomares, E. Energy Levels, Charge Injection, Charge Recombination and Dye Regeneration Dynamics for Donor−acceptor Π-Conjugated Organic Dyes in Mesoscopic TiO_2 Sensitized Solar Cells. *Energy Environ. Sci.* **2011**, *4*, 1820.
(42) Anselmi, C.; Mosconi, E.; Pastore, M.; Ronca, E.; Angelis, F. De Adsorption of Organic Dyes on TiO_2 Surfaces in Dye-Sensitized Solar Cells: Interplay of Theory and Experiment. *Phys. Chem. Chem. Phys.* **2012**, *14*, 15963−15974.
(43) Angelis, F. De; Vitillaro, G.; Kavan, L.; Nazeeruddin, M. K.; Grätzel, M. Modeling Ruthenium-Dye-Sensitized TiO_2 Surfaces Exposing the (001) or (101) Faces: A First-Principles Investigation. *J. Phys. Chem. C* **2012**, *116*, 18124−18131.
(44) Sánchez-de-Armas, R.; Oviedo López, J.; A. San-Miguel, M.; Sanz, J. F.; Ordejón, P.; Pruneda, M. Real-Time TD-DFT Simulations in Dye Sensitized Solar Cells: The Electronic Absorption Spectrum of Alizarin Supported on TiO_2 Nanoclusters. *J. Chem. Theory Comput.* **2010**, *6*, 2856−2865.
(45) Sánchez-de-Armas, R.; San Miguel, M. Á.; Oviedo, J.; Sanz, J. F. Coumarin Derivatives for Dye Sensitized Solar Cells: A TD-DFT Study. *Phys. Chem. Chem. Phys.* **2012**, *14*, 225−233.
(46) Frisch, M. J.; Trucks, G. W.; Schlegel, H. B.; Scuseria, G. E.; Robb, M. A.; Cheeseman, J. R.; Scalmani, G.; Barone, V.; Mennucci, B.; Petersson, G. A.; Nakatsuji, H.; Caricato, M.; Li, X.; Hratchian, H. P.; Izmaylov, A. F.; Bloino, J.; Zheng, G.; Sonnenb, D. J. Gaussian 09, Revision B 01 2009.
(47) Agrawal, S.; Pastore, M.; Marotta, G.; Reddy, M. A.; Chandrasekharam, M.; Angelis, F. De Optical Properties and Aggregation of Phenothiazine-Based Dye-Sensitizers for Solar Cells Applications: A Combined Experimental and Computational Investigation. *J. Phys. Chem. C* **2013**, *117*, 9613−9622.
(48) Pastore, M.; Angelis, F. De Aggregation of Organic Dyes on TiO2 in Dye-Sensitized Solar Cells Models: An Ab Initio Investigation. *ACS Nano* **2010**, *4*, 556−562.
(49) Becke, A. D. Density-Functional Thermochemistry. III. The Role of Exact Exchange. *J. Chem. Phys.* **1993**, *7*, 5648−5652.
(50) Rassolov, V. A.; Ratner, M. A.; Pople, J. A.; Redfern, P. C.; Curtiss, L. A. 6-31G* Basis Set for Third-Row Atoms. *J. Comput. Chem.* **2001**, *22*, 976−984.
(51) Miertuš, S.; Scrocco, E.; Tomasi, J. Electrostatic Interaction of a Solute with a Continuum. A Direct Utilizaion of Ab Initio Molecular Potentials for the Prevision of Solvent Effects. *Chem. Phys.* **1981**, *55*, 117−129.
(52) Dennington, R.; Keith, T.; Millam, J. *GaussView*, version 5; Semichem: Shawnee Mission, KS, 2009.
(53) Turro, N. J. *Modern Molecular Photochemistry*; University Science Books: Sausalito, CA, 1991; p 87.
(54) Vittadini, A.; Selloni, A.; Rotzinger, F. P.; Grätzel, M. Formic Acid Adsorption on Dry and Hydrated TiO_2 Anatase (101) Surfaces by DFT Calculations. *J. Phys. Chem. B* **2000**, *104*, 1300−1306.
(55) Liang, J.; Zhu, C.; Cao, Z. Electronic and Optical Properties of the Triphenylamine-Based Organic Dye Sensitized TiO_2 Semiconductor: Insight from First Principles Calculations. *Phys. Chem. Chem. Phys.* **2013**, *15*, 13844−13851.
(56) Segall, M. D.; Lindan, P. J. D.; Probert, M. J.; Pickard, C. J.; Hasnip, P. J.; Clark, S. J.; Payne, M. C. First-Principles Simulation: Ideas, Illustrations and the CASTEP Code. *J. Phys. Condens. Matter* **2002**, *14*, 2717−2744.
(57) Hagfeldt, A.; Boschloo, G.; Sun, L.; Kloo, L.; Pettersson, H. Dye-Sensitized Solar Cells. *Chem. Rev.* **2010**, *110*, 6595−6663.
(58) Duncan, W. R.; Prezhdo, O. V Theoretical Studies of Photoinduced Electron Transfer in Dye-Sensitized TiO_2. *Annu. Rev. Phys. Chem.* **2007**, *58*, 143−184.
(59) Fantacci, S.; Angelis, F. De A Computational Approach to the Electronic and Optical Properties of Ru(II) and Ir(III) Polypyridyl Complexes: Applications to DSC, OLED and NLO. *Coord. Chem. Rev.* **2011**, *255*, 2704−2726.
(60) Martsinovich, N.; Troisi, A. Theoretical Studies of Dye-Sensitised Solar Cells: From Electronic Structure to Elementary Processes. *Energy Environ. Sci.* **2011**, *4*, 4473.
(61) Martsinovich, N.; Troisi, A. Theoretical Studies of Dye-Sensitised Solar Cells: From Electronic Structure to Elementary Processes. *Energy Environ. Sci.* **2011**, *4*, 4473.
(62) Abbott, L. C.; Batchelor, S. N.; Oakes, J.; Gilbert, B. C.; Whitwood, A. C.; Lindsay Smith, J. R.; Moore, J. N. Experimental and Computational Studies of Structure and Bonding in Parent and Reduced Forms of the Azo Dye Orange II. *J. Phys. Chem. A* **2005**, *109*, 2894−2905.
(63) Liu, X.; Cole, J. M.; Waddell, P. G.; Lin, T.-C.; Radia, J.; Zeidler, A. Molecular Origins of Optoelectronic Properties in Coumarin Dyes: Toward Designer Solar Cell and Laser Applications. *J. Phys. Chem. A* **2012**, *116*, 727−737.
(64) Dean, J. A. *Lange's Handbook of Chemistry*, 15th ed.; McGraw-Hill, Inc.: New York, 1999; pp 91−98.
(65) Zhang, L.; Cole, J. M.; Liu, X. Tuning Solvatochromism of Azo Dyes with Intramolecular Hydrogen Bonding in Solution and on Titanium Dioxide Nanoparticles. *J. Phys. Chem. C* **2013**, *117*, 26316−26323.
(66) Liu, X.; Cole, J. M.; Low, K. S. Molecular Origins of Dye Aggregation and Complex Formation Effects in Coumarin 343. *J. Phys. Chem. C* **2013**, *117*, 14723−14730.
(67) Hagberg, D. P.; Marinado, T.; Karlsson, K. M.; Nonomura, K.; Qin, P.; Boschloo, G.; Brinck, T.; Hagfeldt, A.; Sun, L. Tuning the HOMO and LUMO Energy Levels of Organic Chromophores for Dye Sensitized Solar Cells. *J. Org. Chem.* **2007**, *72*, 9550−9556.
(68) Zeng, W.; Cao, Y.; Bai, Y.; Wang, Y.; Shi, Y.; Zhang, M.; Wang, F.; Pan, C.; Wang, P. Efficient Dye-Sensitized Solar Cells with an Organic Photosensitizer Featuring Orderly Conjugated Ethylenedioxythiophene and Dithienosilole Blocks. *Chem. Mater.* **2010**, *22*, 1915−1925.

(69) Kalyanasundaram, K. *Dye-Sensitized Solar Cells*; EPFL Press: Lausanne, Switzerland, 2010; pp 10−50.
(70) Macrae, C. F.; Edgington, P. R.; McCabe, P.; Pidcock, E.; Shields, G. P.; Taylor, R.; Towler, M.; Streek, J. van de Mercury: Visualization and Analysis of Crystal Structures. *J. Appl. Crystallogr.* **2006**, *39*, 453−457.
(71) Gou, F.; Jiang, X.; Li, B.; Jing, H.; Zhu, Z. Salicylic Acid as a Tridentate Anchoring Group for Azo-Bridged Zinc Porphyrin in Dye-Sensitized Solar Cells. *ACS Appl. Mater. Interfaces* **2013**, *5*, 12631−12637.
(72) Gong, X.-Q.; Selloni, A.; Vittadini, A. Density Functional Theory Study of Formic Acid Adsorption on Anatase TiO_2(001): Geometries, Energetics, and Effects of Coverage, Hydration, and Reconstruction. *J. Phys. Chem. B* **2006**, *110*, 2804−2811.
(73) Liu, X.; Cole, J. M.; Low, K. S. Molecular Origins of Dye Aggregation and Complex Formation Effects in Coumarin 343. *J. Phys. Chem. C* **2013**, *117*, 14723−14730.
(74) El-Zohry, A.; Orthaber, A.; Zietz, B. Isomerization and Aggregation of the Solar Cell Dye D149. *J. Phys. Chem. C* **2012**, *116*, 26144−26153.
(75) Agrawal, S.; Pastore, M.; Marotta, G.; Reddy, M. A.; Chandrasekharam, M.; Angelis, F. De Optical Properties and Aggregation of Phenothiazine-Based Dye-Sensitizers for Solar Cells Applications: A Combined Experimental and Computational Investigation. *J. Phys. Chem. C* **2013**, *117*, 9613−9622.
(76) Pastore, M.; Angelis, F. De Aggregation of Organic Dyes on TiO_2 in Dye-Sensitized Solar Cells Models: An Ab Initio Investigation. *ACS Nano* **2010**, *4*, 556−562.
(77) Rochford, J.; Chu, D.; Hagfeldt, A.; Galoppini, E. Tetrachelate Porphyrin Chromophores for Metal Oxide Semiconductor Sensitization: Effect of the Spacer Length and Anchoring Group Position. *J. Am. Chem. Soc.* **2007**, *129*, 4655−4665.
(78) Sánchez-de-Armas, R.; San-Miguel, M. A.; Oviedo, J.; Sanz, J. F. Molecular Modification of Coumarin Dyes for More Efficient Dye Sensitized Solar Cells. *J. Chem. Phys.* **2012**, *136*, 194702.
(79) Ozawa, H.; Awa, M.; Ono, T.; Arakawa, H. Effects of Dye-Adsorption Solvent on the Performances of the Dye-Sensitized Solar Cells Based on Black Dye. *Chem.—Asian J.* **2012**, *7*, 156−162.
(80) Kim, S.; Lee, J. K.; Kang, S. O.; Ko, J.; Yum, J.-H.; Fantacci, S.; De Angelis, F.; Di Censo, D.; Nazeeruddin, M. K.; Grätzel, M. Molecular Engineering of Organic Sensitizers for Solar Cell Applications. *J. Am. Chem. Soc.* **2006**, *128*, 16701−16707.
(81) Meyer, T.; Ogermann, D.; Pankrath, A.; Kleinermanns, K.; Müller, T. J. J. Phenothiazinyl Rhodanylidene Merocyanines for Dye-Sensitized Solar Cells. *J. Org. Chem.* **2012**, *77*, 3704−3715.
(82) Miguel, G. de; Ziółek, M.; Zitnan, M.; Organero, J. A.; Pandey, S. S.; Hayase, S.; Douhal, A. Photophysics of H- and J-Aggregates of Indole-Based Squaraines in Solid State. *J. Phys. Chem. C* **2012**, *116*, 9379−9389.
(83) Ooyama, Y.; Harima, Y. Molecular Designs and Syntheses of Organic Dyes for Dye-Sensitized Solar Cells. *European J. Org. Chem.* **2009**, *2009*, 2903−2934.
(84) Li, S.-F.; Yang, X.-C.; Cheng, M.; Zhao, J.-H.; Wang, Y.; Sun, L.-C. Novel D−π−A Type II Organic Sensitizers for Dye Sensitized Solar Cells. *Tetrahedron Lett.* **2012**, *53*, 3425−3428.
(85) He, H.; Gurung, A.; Si, L. 8-Hydroxylquinoline as a Strong Alternative Anchoring Group for Porphyrin-Sensitized Solar Cells. *Chem. Commun.* **2012**, *48*, 5910−5912.
(86) An, B.-K.; Hu, W.; Burn, P. L.; Meredith, P. New Type II Catechol-Thiophene Sensitizers for Dye-Sensitized Solar Cells. *J. Phys. Chem. C* **2010**, *114*, 17964−17974.
(87) Yan, Z.; Guang, S.; Su, X.; Xu, H. Near-Infrared Absorbing Squaraine Dyes for Solar Cells: Relationship between Architecture and Performance. *J. Phys. Chem. C* **2012**, *116*, 8894−8900.
(88) Ooyama, Y.; Nagano, T.; Inoue, S.; Imae, I.; Komaguchi, K.; Ohshita, J.; Harima, Y. Dye-Sensitized Solar Cells Based on Donor-Π-Acceptor Fluorescent Dyes with a Pyridine Ring as an Electron-Withdrawing-Injecting Anchoring Group. *Chem.—Eur. J.* **2011**, *17*, 14837−14843.
(89) Ooyama, Y.; Inoue, S.; Asada, R.; Ito, G.; Kushimoto, K.; Komaguchi, K.; Imae, I.; Harima, Y. Dye-Sensitized Solar Cells Based on a Novel Fluorescent Dye with a Pyridine Ring and a Pyridinium Dye with the Pyridinium Ring Forming Strong Interactions with Nanocrystalline TiO2 Films. *Eur. J. Org. Chem.* **2010**, *2010*, 92−100.
(90) Ooyama, Y.; Yamaguchi, N.; Imae, I.; Komaguchi, K.; Ohshita, J.; Harima, Y. Dye-Sensitized Solar Cells Based on D-π-A Fluorescent Dyes with Two Pyridyl Groups as an Electron-Withdrawing-Injecting Anchoring Group. *Chem. Commun.* **2013**, *49*, 2548−2550.
(91) Daphnomili, D.; Landrou, G.; Prakash Singh, S.; Thomas, A.; Yesudas, K.; K, B.; Sharma, G. D.; Coutsolelos, A. G. Photophysical, Electrochemical and Photovoltaic Properties of Dye Sensitized Solar Cells Using a Series of Pyridyl Functionalized Porphyrin Dyes. *RSC Adv.* **2012**, *2*, 12899.
(92) Zhang, M.-D.; Xie, H.-X.; Ju, X.-H.; Qin, L.; Yang, Q.-X.; Zheng, H.-G.; Zhou, X.-F. D-D-Π-A Organic Dyes Containing 4,4′-di(2-Thienyl)triphenylamine Moiety for Efficient Dye-Sensitized Solar Cells. *Phys. Chem. Chem. Phys.* **2013**, *15*, 634−641.
(93) Daphnomili, D.; Sharma, G. D.; Biswas, S.; Justin Thomas, K. R.; Coutsolelos, A. G. A New Porphyrin Bearing a Pyridinylethynyl Group as Sensitizer for Dye Sensitized Solar Cells. *J. Photochem. Photobiol. A Chem.* **2013**, *253*, 88−96.
(94) Lu, J.; Xu, X.; Li, Z.; Cao, K.; Cui, J.; Zhang, Y.; Shen, Y.; Li, Y.; Zhu, J.; Dai, S.; et al. Zinc Porphyrins with a Pyridine-Ring-Anchoring Group for Dye-Sensitized Solar Cells. *Chem.—Asian J.* **2013**, *8*, 956−962.
(95) Harima, Y.; Fujita, T.; Kano, Y.; Imae, I.; Komaguchi, K.; Ooyama, Y.; Ohshita, J. Lewis-Acid Sites of TiO_2 Surface for Adsorption of Organic Dye Having Pyridyl Group as Anchoring Unit. *J. Phys. Chem. C* **2013**, *117*, 16364−16370.